Physical interactions reduce the power of natural selection in growing yeast colonies

Andrea Giometto[a,b,c,1], David R. Nelson[a,b,c,d], and Andrew W. Murray[b,c,1]

[a]Department of Physics, Harvard University, Cambridge, MA 02138; [b]Faculty of Arts and Sciences Center for Systems Biology, Harvard University, Cambridge, MA 02138; [c]Department of Molecular and Cellular Biology, Harvard University, Cambridge, MA 02138; and [d]School of Engineering and Applied Sciences, Harvard University, Cambridge, MA 02138

Contributed by Andrew W. Murray, September 17, 2018 (sent for review June 5, 2018; reviewed by Terence Hwa and Boris I. Shraiman)

Microbial populations often assemble in dense populations in which proliferating individuals exert mechanical forces on the nearby cells. Here, we use yeast strains whose doubling times depend differently on temperature to show that physical interactions among cells affect the competition between different genotypes in growing yeast colonies. Our experiments demonstrate that these physical interactions have two related effects: they cause the prolonged survival of slower-growing strains at the actively-growing frontier of the colony and cause faster-growing strains to increase their frequency more slowly than expected in the absence of physical interactions. These effects also promote the survival of slower-growing strains and the maintenance of genetic diversity in colonies grown in time-varying environments. A continuum model inspired by overdamped hydrodynamics reproduces the experiments and predicts that the strength of natural selection depends on the width of the actively growing layer at the colony frontier. We verify these predictions experimentally. The reduced power of natural selection observed here may favor the maintenance of drug-resistant cells in microbial populations and could explain the apparent neutrality of interclone competition within tumors.

spatial population genetics | selective sweep | range expansion | evolution | extinction

Life in the microbial world often occurs in crowded environments, such as colonies, biofilms, and tissues. Within these dense populations, cells compete for nutrients and space to survive, proliferate, and propagate their genotype. Classical results of population genetics theory on the competition between genotypes in well-mixed populations (1) do not apply directly to these microbial aggregates, due to their growing size and spatial structure (2–9). Microbial range expansion experiments are a valuable tool for investigating ecological and evolutionary dynamics in spatial contexts (4, 5, 10–15) and extend our understanding of spatial population genetics (16). Early studies of microbial range expansions have shown that the growth of microbial colonies causes the spatial separation of genotypes (2), which makes theoretical models derived for well-mixed populations inapplicable. Biological interactions between genotypes can either reduce this segregation or increase it, depending on the nature of the interactions. For instance, Müller et al. (10) showed that mutualistic yeast strains cannot demix if they are obligate mutualists and thus depend on each other for growth. In contrast, McNally et al. (17) showed that antagonistic interactions among bacterial strains cause a phase separation that increases the spatial separation of different strains. Although additional deviations from classical theory could be produced by the mechanical interaction between cells in dense populations, the effects of such interactions on microbial competition are still relatively unexplored. Among the few exceptions, Farrell et al. (18) showed that the physical properties of cells can affect the dynamics of beneficial mutations in growing colonies. They showed that the probability that a mutant spreads in the population can be related to summary statistics characterizing cell alignment and the front roughness. In parallel to our investigation, Kayser et al. (19) showed that the mechanical interaction between a faster-growing and a slower-growing strain can cause the prolonged survival of the slower-growing one at the colony frontier, a process that we have investigated in a different geometry and from a different modeling perspective.

In this work, we study the effect of mechanical interactions among cells on the competition of strains in growing colonies of the budding yeast, *Saccharomyces cerevisiae*. We focus on the competition for space and for nutrients of two yeast strains with different fitnesses and study the dynamics of selective sweeps (the fitter strain's increase in relative frequency at the frontier of the expanding colony) and the local extinction dynamics of the less-fit strain. In *S. cerevisiae* colonies, growth occurs mostly in close proximity to the outer boundary, and so we consider a strain to be extinct if it lags behind during the expansion and exits the growth zone. We find that mechanical interactions reduce the strength of natural selection by slowing down the extinction of slower-growing strains and by reducing the rate at which faster-growing ones increase their frequency. We show that a continuum model inspired by overdamped hydrodynamics can reproduce the experimental data and make predictions that we verify experimentally. Specifically, the model predicts that the speed at which selective sweeps spread in a growing colony is inversely related to the width of the actively growing layer at the colony frontier. We tested the model by coculturing two yeast strains with different temperature-dependent growth profiles. We show that the prolonged survival of the less-fit strain, which occurs via the formation of thin, persistent filaments (Fig. 1 *A*–*A2*), promotes the maintenance of genetic diversity in the population when two strains compete in an environment in which their relative growth rates vary with time. This reduction in the

Significance

Microbes often live in dense populations such as colonies and biofilms. We show that the success and extinction of yeast strains within a growing colony are determined by a combination of their relative fitness and the forces exerted by proliferating cells on their neighbors. These physical interactions prolong the survival of less-fit strains at the growing frontier of the colony and slow down the colony's takeover by fitter strains. This reduction in the power of natural selection favors the maintenance of genetic diversity in environments in which the strains' relative growth rates vary with time. Growth-induced physical interactions may thus favor the maintenance of drug-resistant cells, which are typically less fit than non-resistant cells, within dense microbial populations.

Author contributions: A.G., D.R.N., and A.W.M. designed research; A.G. performed research; A.G. analyzed data; and A.G., D.R.N., and A.W.M. wrote the paper.

Reviewers: T.H., University of California, San Diego; and B.I.S., University of California, Santa Barbara.

The authors declare no conflict of interest.

[1]To whom correspondence may be addressed. Email: andrea.giometto@gmail.com or awm@mcb.harvard.edu.

This article contains supporting information online at www.pnas.org/lookup/suppl/doi:10.1073/pnas.1809587115/-/DCSupplemental.

Published online October 23, 2018.

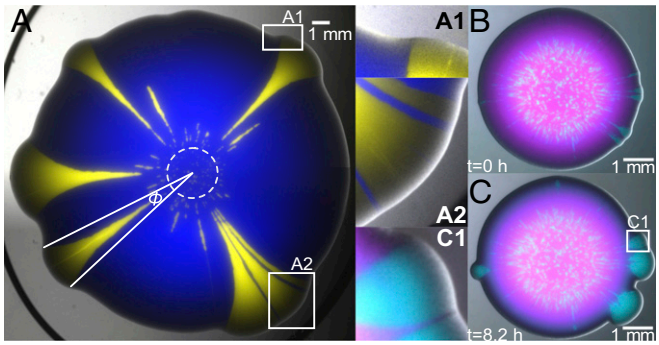

Fig. 1. *S. cerevisiae* colony-growth experiments hint at physical interactions between strains. (*A*) Combined fluorescent and bright-field image of a colony, 4 d after the inoculation of a mixed droplet of strains yAG1 (blue) and yAG2 (yellow) at relative frequencies of 99% and 1%, grown at 30 °C. The white dashed circle marks the inoculum size. Because yAG2 divides faster at 30 °C, some single-strain yellow sectors expand their opening angle ϕ as the colony grows radially, while others go extinct due to stochastic effects in the early stages of growth. By expanding faster, the faster-growing strain displaces the other strain at both sides of yellow sectors (*A1*) and can enhance the expansion speed of the slower-growing strain when it is trapped between two yellow sectors (blue filaments in *A2*) and is carried along. (*B* and *C*) Even nonproliferating cells (magenta) can be pulled outward by a proliferating (cyan) strain. The images show combined fluorescent and bright-field images of the same colony at early and later times. In this experiment, the non–heat-sensitive strain yAG19 (cyan, initial frequency 10%) and the heat-sensitive strain yAG20 (magenta, initial frequency 90%) were grown at 28 °C for 2 d and subsequently imaged with a stereoscope incubated at 37 °C, a temperature at which yAG20 cells cannot divide. *B* shows the first snapshot at which the heat-sensitive strain stopped expanding (*SI Appendix*, Fig. S1*D*). *C* shows the colony after a further 8.2 h. (*C1*) Close-up of the region marked with a white square in *C*, highlighting the displacement of the nongrowing, heat-sensitive strain next to expanding sectors of the growing strain and an expanding magenta filament trapped between two cyan sectors. Because the heat-sensitive strain did not divide between *B* and *C*, its displacement is due to the physical interaction between the two strains.

efficiency of natural selection may be beneficial for microbial populations by delaying the extinction of slower-growing cells which carry traits that can later be beneficial for the population, such as drug resistance.

Results

When two yeast strains are mixed and inoculated as a drop on a solid nutrient medium, they form a mixed-strain colony that expands radially with time. A well-known feature of such colony expansion is the spatial demixing of strains due to genetic drift (2), which forms single-strain sectors. When one strain expands faster than the other, the size of its sectors increases with time (5) (Fig. 1*A*). We performed colony-growth experiments using two *S. cerevisiae* strains with different doubling times. As expected, single-strain colonies of the strain (yAG2) with the larger growth rate ($\bar{g}_2 = 0.42 \pm 0.05$ h^{-1}, median ± SD) expanded faster than single-strain colonies of the strain (yAG1) with the smaller growth rate ($\bar{g}_1 = 0.38 \pm 0.06$ h^{-1}, median ± SD). We found that single-strain sectors within mixed colonies interact mechanically in ways that affect the competition between the two strains. These mechanical interactions are visible in Fig. 1*A*. At each side of sweeping sectors of the faster-growing (yellow) strain, the slower-growing (blue) strain was displaced and pulled toward the exterior of the colony (Fig. 1 *A* and *A1*). Occasionally, the slower-growing strain was trapped between two sectors of the faster-growing one in the early phases of the expansion and traveled longer distances (blue filaments in Fig. 1 *A*–*A2*) than in other regions of the colony, where the slower-growing strain was farther from the faster-growing strain. The enhanced expansion of the slower-growing strain occurs as a thin, persistent filament (composed of several thousand cells, not to be confused with bacterial filamentous cells) that originates via a combination of cell division and the physical interactions with the faster-growing strain.

We wanted to rule out the possibility that persistent filaments were due to the ability of the faster-growing strain to speed up (for example, via chemical secretions) the proliferation of cells of the slower-growing strain that were nearby. We therefore produced mixed colonies from two strains: a wild-type strain that proliferated at temperatures from 20 to 37 °C (yAG19, cyan in Fig. 1 *B* and *C*) and a strain carrying a temperature-sensitive mutation that could only proliferate at temperatures below 30 °C (yAG20, magenta in Fig. 1 *B* and *C*). To ask if the formation of persistent filaments required the proliferation of the less-fit strain, we imposed the extreme condition of preventing the proliferation of the less-fit strain. The heat-sensitive strain used here is a *cdc26Δ* mutant that arrests in mitosis and therefore cannot complete the cell division cycle at temperatures above 30 °C (20). We grew single-strain and mixed-strain colonies of these two strains at 28 °C for 2 d and subsequently imaged them with a stereoscope incubated at 37 °C for 23 h. We observed that single-strain, heat-sensitive colonies stopped expanding after 9 h from the start of the measurement (Fig. 1*B* and *SI Appendix*, Fig. S1). In the following hours, single-strain sectors of the non–heat-sensitive strain emerged from the mixed colony, displacing the heat-sensitive strain and producing patterns (Fig. 1 *C* and *C1*) that are visually similar to those shown in Fig. 1*A*. Specifically, the nondividing heat-sensitive strain was nevertheless displaced on each side of sweeping sectors of the non–heat-sensitive one and sectors of the heat-sensitive strain trapped between two sectors of the other strain (Fig. 1*C1*, *SI Appendix*, Fig. S2, and Movie S1) were squeezed and formed filaments that resemble those shown in Fig. 1 *A*–*A2*. Because the heat-sensitive single-strain colonies were not expanding when non–heat-sensitive sectors emerged from the mixed-strain colony (*SI Appendix*, Fig. S1*D*), the displacement of the heat-sensitive strain was caused by the physical interaction between the two strains and the formation of thin filaments did not require the proliferation of the less-fit strain.

The experiments described above show that mechanical interactions cause the prolonged survival of the slower-growing strain, via thin, persistent filaments trapped between sectors of the faster-growing strain. To highlight the effect of this persistence on the competitive dynamics of strains in growing colonies, we designed a colony-growth experiment in which we could use environmental switches to alternate which strains grew faster and slower. The strain yAG2 is cold-sensitive due to the *trp1-1* mutation, which requires it to import tryptophan from the medium, a process whose efficiency is reduced at low temperatures (21), so that yAG1 grows faster than yAG2 at low temperatures and more slowly at high temperatures. At 12 °C, single-strain colonies of yAG1 expanded faster (0.288 ± 0.004 mm/d) than those of yAG2 (0.23 ± 0.01 mm/d), whereas at 30 °C single-strain colonies of yAG2 expanded faster (1.15 ± 0.02 mm/d) than those of yAG1 (0.96 ± 0.03 mm/d). Thus, by changing the temperature during a mixed-strain colony-growth experiment, we could control which strain was proliferating faster. We performed mixed-strain colony-growth experiments starting from a 50–50% mixture of the two strains and incubated them at 30 °C at the start of the experiment, then moved the colonies to 12 °C after a few days, and moved them again to 30 °C toward the end of the experiment (*Methods*). The duration of each temperature phase varied between replicates. Fig. 2 and *SI Appendix*, Figs. S3–S5 show that strains can survive as persistent, thin filaments at the temperature where they grow slower and then expand in the next phase, at a temperature where they grow faster than their competitor.

We made a hydrodynamic model to describe the observed interactions between strains at the macroscopic scale (i.e., at scales much larger than the typical cell diameter). Our model for the dynamics of the competition between two strains in growing colonies used a 2D continuum description based on overdamped hydrodynamics. This approach is valid on time scales that are long compared with a cell division time and length scales that are large compared with a cell diameter and to the colony height near the frontier. We first describe the model for a single-strain colony and then generalize it to the case of multiple strains. Let

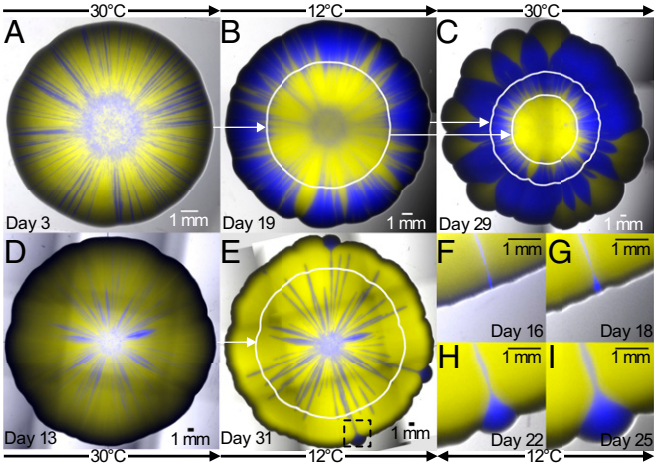

Fig. 2. Colony-growth experiments in time-varying environments highlight the relevance of mechanical interactions to the competition between strains in mixed colonies. (*A*) Mixed yAG1 (blue, 50% initial frequency, the faster-growing strain at 12 °C) and yAG2 (yellow, 50% initial frequency, the faster-growing strain at 30 °C) colony grown at 30 °C for 3 d. The colony was then grown for 16 d at 12 °C (*B*) and for further 10 d at 30 °C (*C*). (*D*) A different, mixed yAG1 (blue, 50% initial frequency) and yAG2 (yellow, 50% initial frequency) colony grown at 30 °C for 13 d. The colony was then grown for 18 d at 12 °C (*E*). At each temperature, the slower-growing strain survives as thin, persistent filaments that allow it to recover at the colony frontier following temperature changes. White curves show the colony perimeter at the previous temperature switch. Pictures were taken immediately before temperature changes (*A*, *B*, and *D*) and at the end of the experiments (*C* and *E*). *F*–*I* show the recovery of the strain yAG1 (in the region corresponding to the black, dashed square in *E*) from a thin filament during growth at 12 °C. Temperatures shown indicate the incubation temperature during the days immediately preceding the images. The colony sizes are rescaled to be approximately equal in radius.

$\rho(x,y,t)$ be the 2D density (with dimensions of cells per length squared) of a single-strain colony at time t, where x and y are Cartesian coordinates on the agar plane. If h is the height of the colony, we have $\rho = h\rho_{3d}$, where we assume that the 3D density ρ_{3d} (with dimensions of cells per length cubed) is constant within the colony. Colony expansion in the vertical direction is much slower than the expansion in the horizontal plane of the agar and thus experimental colonies are approximately flat in the direction parallel to the agar surface. We therefore assume that h (and thus ρ) is also constant within the colony, and equal to zero outside. Let $g(x,y,t)$ be the local growth rate (with dimensions of 1/time) of yeast cells in position (x,y) at time t. Experimental observations reveal that the 2D spatial distribution of strains in mixed-strain colonies is approximately time-invariant at distances larger than 500 μm (about 100 cell diameters) behind the colony frontier (*SI Appendix*, section 9), indicating that cell divisions that affect the visible surface of the colony take place mostly within this distance from the frontier. This observation led us to define a distance δ from the frontier of the colony such that $g(x,y,t) = \bar{g}$, with constant $\bar{g} > 0$, for every point (x,y) inside the colony within a distance δ from the frontier at time t, and $g(x,y,t) = 0$ for every other point. From a hydrodynamic perspective, cell growth is seen as a source of fluid with space- and time-dependent rate g. With these assumptions, the radial expansion speed of a circular single-strain colony is equal to $\bar{v} = dr/dt = \bar{g}\delta[1 - \delta/(2r)] \cong \bar{g}\delta$ (*SI Appendix*, *Supplementary Methods*), where the last approximation is justified because typically $\delta \ll r$ in colony-growth experiments. The 2D velocity $\vec{v}(x,y,t)$ which displaces cells within the colony satisfies

$$\vec{\nabla} \cdot \vec{v} = g, \qquad [1]$$

where $\vec{\nabla} \cdot \vec{v}$ is the divergence of $\vec{v}$. Eq. 1 enforces mass conservation within the colony along a streamline, ensuring that the 2D density ρ is constant inside the colony. Within the colony, the 2D pressure field $p(x,y,t)$ satisfies the equation

$$\vec{\nabla} p = -\gamma \vec{v}, \qquad [2]$$

which states that the velocity $\vec{v}$ is proportional to the pressure gradient $\vec{\nabla} p$ and inversely proportional to γ, the frictional drag applied to the colony by the substrate. Eqs. 1 and 2 have been used previously to model biofilm growth (22). We show in *SI Appendix*, section 3 that they can be derived from the 3D continuity and Navier–Stokes equations by adopting the lubrication approximation (23), which gives the value of the friction coefficient $\gamma = 2\mu/h^2$ in terms of the colony dynamic viscosity μ and the colony height h. The approximation is appropriate when $\sqrt{2}\delta/h \gg 1$, that is, when the height of the colony is small compared with the growth-layer width, as found experimentally ($\sqrt{2}\delta/h \cong 10$–$35$, depending on the experimental setup). Upon taking the divergence of Eq. 2 and using Eq. 1, one finds:

$$\nabla^2 p = -\gamma \vec{\nabla} \cdot \vec{v} = -\gamma g, \qquad [3]$$

that is, the pressure field within the colony satisfies a Poisson equation, with the boundary condition $p = p_0$ at the outer edge of the colony, where p_0 is a constant reference pressure (because the value of p_0 does not affect the dynamics, we set $p_0 = 0$). This simple model can be generalized to mixed-strain colonies by considering two different 2D densities $\rho_1(x,y,t)$ and $\rho_2(x,y,t)$, giving the density of each strain. Given the sharp boundaries between the two strains observed in colony-growth experiments (see, e.g., Fig. 1*A*), we assume that the two strains cannot simultaneously occupy the same position in space at the same time t, so that for each point (x,y) within the colony either ρ_1 or ρ_2 must be equal to zero, and the colony density is equal to $\rho = \rho_1 + \rho_2$. In the same way, the local growth rate is equal to $g = g_1 + g_2$ within the colony, where either g_1 or g_2 must be equal to zero, according to which strain occupies the position (x,y) at time t. With this definition of g, the velocity field and pressure in the mixed-strain model are still given by Eqs. 2 and 3. Note that, because pressure is proportional to γ (Eq. 3) and the velocity field is given by $\vec{v} = -\vec{\nabla} p/\gamma$ (Eq. 2), the frictional coefficient γ drops out and its value does not affect the displacement of strains within the colony and thus its spatiotemporal dynamics. Even though growth is localized within a layer of width δ at the colony frontier, the velocity field given by Eq. 2 will in general be nonzero in the interior of the colony. However, the velocity modulus decreases sharply with the distance from the frontier and is negligible outside the growth layer (Fig. 3*D*), so that flow in the colony occurs mostly within the growth layer.

We find that simulations based on this continuum model can reproduce the experimental observation of the mechanical interaction of single-strain sectors within growing colonies (Fig. 3*B*), namely the displacement of the slower-growing strain in the proximity of a faster-growing sector and the prolonged survival and enhanced expansion speed of thin filaments of the slower-growing strain trapped between two sectors of the faster-growing one (Fig. 3*B*). Both these effects become more pronounced as the width, δ, of the growth layer increases. Note that the same observations are not predicted by a constant-speed model (5) inspired by geometrical optics in which each strain advances at a constant speed, perpendicular to the frontier of the colony (Fig. 3*A*). The constant-speed model is known to fail for the early dynamics of sweeping sectors (e.g., for sectors composed of cells with beneficial mutations), for example when the two walls bounding such sectors are close to each other (5). The temporal dynamics of a sweeping sector can be quantified by its opening angle, which is defined as the angle formed by the two lines connecting the center of the inoculum to the boundary between the

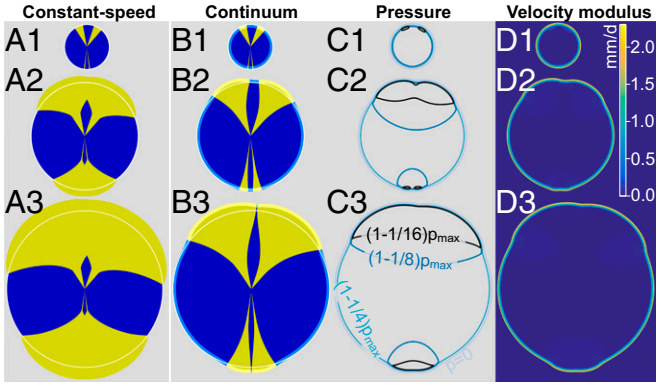

Fig. 3. The constant-speed model inspired by geometrical optics (*A1–A3*) and the continuum model (*B1–B3*) make different predictions for the competition of yeast strains in growing colonies. Both models were integrated numerically, starting from the same initial condition shown in *A1* and *B1*. The constant-speed model (*A1–A3*) fails to reproduce the thin, persistent filaments observed experimentally (Fig. 1 *A–A2*), but such filaments are seen for the blue strain in the continuum model (*B1–B3*). The opening angle of yellow sectors increases faster in the constant-speed model (*A1–A3*) than in the continuum model (*B1–B3*), consistent with the experimental observations in Fig. 4. White contours are circles fit to the blue-strain outer profile far from yellow sectors; they highlight the displacement of the blue strain close to yellow sectors in the continuum model. The growth layer is shown in *B1–B3* using light-yellow and light-blue colors. *C1–C3* show pressure contours $p = 0$ and $(1 - 1/n)p_{\max}$, where $n = 4, 8, 16$ and $p_{\max}$ was evaluated at each time step. *D1–D3* show the local velocity modulus in the continuum model simulations and highlight that the displacement of strains takes place mostly within the growth layer. Model parameters are $\bar{v}_1 = 1.89$ mm/d, $\bar{v}_2 = 2.33$ mm/d, and $\delta = 290$ μm.

two strains at the frontier of the colony (e.g., the angle ϕ in Fig. 1*A*). In the constant-speed model, the sector boundaries form logarithmic spirals, with their opening angle increasing logarithmically with the radius of the colony (5). In simulations of the continuum model, however, the dynamics of opening angles can be separated into two stages, which are best seen on a log-linear scale (continuous lines in Fig. 4*D*). Initially, opening angles increase exponentially with the radius r, defined at the point in which the two strains meet at the frontier of the colony (Fig. 4*A*, *Inset*). At later times (or, equivalently, larger radii r), the rate of increase of sweeping sector opening angles versus r eventually tends to the constant-speed model prediction (Fig. 4*D* and *SI Appendix*, Fig. S9), that is, opening angles increase logarithmically with r. We find that the continuum model results tend to the constant-speed model ones as the width of the growth layer δ tends to zero, while keeping the constant asymptotic expansion speed $\bar{v}_i = \bar{g}_i\delta$ of each strain i constant by varying $\bar{g}_i$ (*SI Appendix*, Fig. S9). This observation makes sense because the constant-speed model, which is inspired by geometrical optics, assumes that each point at the colony frontier (corresponding to an extremely narrow growth layer) is the source of a circular growth wave in the infinitesimal time interval dt, and that the outline of the colony at time $t + dt$ is given by the envelope of such waves (5).

We tested whether our continuum model could reproduce the observed temporal evolution of the opening angles of sweeping sectors. We performed colony-growth experiments at 30 °C with the slower-growing strain yAG1 and the faster-growing strain yAG2 and measured the opening angles of sweeping yAG2 sectors that remained far from each other throughout the entire experiment (e.g., the four isolated yellow sectors at 2, 8, 9, and 11 o'clock in Fig. 1*A*). Opening angles measured at different times and colony radii are shown in Fig. 4 *A* and *B* and *SI Appendix*, Fig. S10. We grouped the experimentally measured opening angle trajectories of sweeping yAG2 sectors into two classes (small and large angles), based on the opening angle of each sector at the second measurement point, which was taken as the initial condition for the comparison with the models (see *SI Appendix*, section 7 for an explanation). A log-linear plot highlights the initial exponential dependence of opening angles on the distance from the center of the colony to the points at which yAG1 and yAG2 sectors meet at the frontier of the colony (Fig. 4*B*). The constant-speed model (dashed lines in Fig. 4 *A* and *B*, based on each strain's expansion velocity measured in single-strain colony growth experiments), strongly overestimates the initial increase in the opening angles of sweeping yAG2 sectors. We tested if our continuum model could reproduce the experiments by fitting the continuum model to the experimental opening angles of sweeping sectors. The expansion velocities $\bar{v}_1$ and $\bar{v}_2$ measured in single-strain colony-growth experiments (*SI Appendix*, section 8 and Fig. S11) constrained the products $\bar{g}_1\delta = \bar{v}_1$ and $\bar{g}_2\delta = \bar{v}_2$ in the continuum model, assuming an identical growth-layer width δ for the two strains. Thus, we could vary the width δ of the growth layer in the model ($\bar{g}_1$ and $\bar{g}_2$ were then uniquely determined) and use it as a parameter to fit the sector opening angles. The resulting model fit is shown in Fig. 4 *A* and *B* (continuous lines). The best-fit estimate is $\delta = 290$ μm (68% CI [260, 350] μm). We experimentally measured the characteristic length scale over which growth affects the visible surface of yeast colonies and found it to be equal to $\delta_{\exp} = 530 \pm 120$ μm (mean ± SD; see *SI Appendix*, section 9 and Fig. S12). The best-fit estimate of δ is smaller than δ_{exp}, but this is not surprising given that the colony height goes to zero at the colony frontier, whereas the model assumes constant height everywhere (geometrical considerations suggest that $\delta_{exp} = 2\delta$; see *SI Appendix*, section 9).

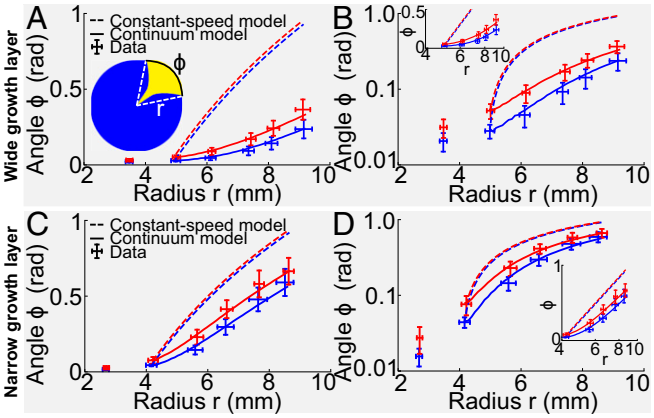

Fig. 4. Dynamics of sector opening angles (data points are mean ± SD) of strain yAG2 opening into strain yAG1 at 30 °C after the inoculation of mixed-strain colonies with yAG2 relative frequency of 1%. (*A*, *Inset*) A sketch of a sweeping sector. The radius r is defined as the distance from the center of the colony to the point at which the two strains meet at the frontier (dashed, white lines). The sector opening angle ϕ is the angle formed by the dashed, white lines, subtended by the arc shown in black. Experimental data were divided in two classes with equal numbers of sectors, based on the opening angle at the second measurement point (blue: small angle, red: large angle, *SI Appendix, Supplementary Methods*). Dashed curves are predictions of the constant-speed model. Continuous curves are best fits to the continuum model. (*A*) Sector dynamics (red: 27 sectors, blue: 27 sectors) of the fitter strain in colonies with a wide layer of active growth at the frontier. (*B*) Same as *A* in log-linear scale. (*Inset*) Same data (with radii ≥ 4 mm) in linear-log scale, where the constant-speed model prediction is a straight line. (*C* and *D*) Same as *A* and *B* for sector dynamics in colonies with a narrow layer of active growth at the frontier (red: 10 sectors, blue: 10 sectors). Experimental data show that opening angles increase more rapidly for narrow growth layers (*C* and *D*) than for wider ones (*A* and *B*). The transition between the exponential and logarithmic growth of opening angles with the radius r is clearly visible in *D*. The constant-speed model (dashed lines) cannot reproduce the initial opening angles dynamics. The continuum model (continuous lines), on the other hand, can reproduce the data, using the growth-layer width δ as a parameter. In *A* and *B*, the best-fit parameter was $\delta = 290$ μm and in *C* and *D* it was $\delta = 110$ μm.

The continuum model predicts that the opening angles of sweeping sectors increase faster for smaller values of δ. To test this prediction, we reduced the value of the growth-layer width δ by reducing the wetness of the agar plates and measured the dynamics of the opening angles of sweeping sectors in this condition (Fig. 4 *C* and *D*). We experimentally verified that the growth-layer width was reduced, compared with wetter plates (*SI Appendix*, section 9 and Fig. S12). In the experiment with a narrower growth-layer width, even though the ratio of the expansion velocities of the two single strains ($\bar{v}_2/\bar{v}_1 = 1.17 \pm 0.06$) was slightly smaller than in the experiment with wider growth-layer width ($\bar{v}_2/\bar{v}_1 = 1.23 \pm 0.05$), the opening angles increased more rapidly, consistent with the smaller growth-layer width δ, thus verifying the continuum model's prediction. Although the constant-speed model fails to predict correctly the early time dynamics of opening angles, it does a better job than for the previous experiment, as expected given the smaller value of δ and our observation that the continuum model tends to the constant-speed model in the limit $\delta \to 0$. As in the previous experiment, our continuum model can reproduce the experimental dynamics of sweeping sector opening angles by fitting the growth-layer width to the data (Fig. 4 *C* and *D*, continuous lines). The best-fit parameter for this experiment is $\delta = 110 \pm 20$ μm. In this case, one can observe the transition from the exponential (for small ϕ and small r) to logarithmic dependence of ϕ on r predicted by our continuum model (Fig. 4 *C* and *D*). Such a transition is not discernible (or barely so) in the experiment described in the previous paragraph (Fig. 4 *A* and *B*), due to the larger value of the growth-layer width δ for wetter plates. In both experiments, the ratio $\bar{v}_2/\bar{v}_1$ matches the ratio of experimentally measured growth rates ($\bar{g}_2/\bar{g}_1 = 1.19 \pm 0.06$, mean ± SE), as expected based on the model prediction for the asymptotic expansion speed $\bar{v} = \bar{g}\delta$.

Discussion

Our experiments show that physical (pressure-induced) interactions between yeast strains within growing colonies reduce the efficiency of natural selection both by allowing less-fit strains to persist and by slowing down the expansion of fitter strains. Slower-growing strains expand faster in parts of the colony that are close to faster-growing strains. When a slower-growing strain is trapped in a thin gap between two sectors of the faster-growing one, it expands at almost the same speed as the latter and forms a persistent, thin filament that can survive for very long times. A geometrical, toy model which neglects the contribution of curvature to the front propagation velocity (*SI Appendix*, section 10) suggests that the thickness of these filaments decreases exponentially over a typical length scale $l = \delta(1 - \bar{v}_1/\bar{v}_2)^{-1}$, which increases with increasing growth-layer width δ and the ratio $\bar{v}_1/\bar{v}_2 = \bar{g}_1/\bar{g}_2$. In the experiments, we found that thin filaments can persist longer than initially larger sectors of the slower-growing strain, which are usually pinched off by sectors of the faster-growing strain that meet each other at the frontier of the colony subtending a substantial angle (*SI Appendix*, section 11 and Fig. S15). The prolonged survival of thin, persistent filaments is favored by the small fluctuations of the filament boundaries relative to the filament thickness (*SI Appendix*, section 12 and Fig. S16). Physical interactions also slow the initial dynamics of selective sweeps compared with the expectation of the constant-speed model, which assumes that the strains expand independently of each other except that two strains cannot occupy the same position. The magnitude of these effects increases with the width δ of the actively growing layer at the frontier of the expanding colony. Our continuum model gives us an intuition for the physical origin of the experimental observations. Thin, persistent filaments are pushed toward the exterior of the colony by the surrounding faster-growing strain and benefit from the pressure field generated by the latter. Conversely, sweeping sectors of the faster-growing strain that have small initial opening angles are too small to generate enough pressure and thus initially expand more slowly than the predictions of the constant-speed model. Even though our continuum model is deterministic and thus cannot reproduce the stochastic extinction of small sectors of the faster-growing strain, which are sometimes observed in the experiments (see, e.g., Fig. 1*A*), it helps us to understand why such extinctions can occur. Sectors of the faster-growing strain initially expand at approximately the same speed as the surrounding slower-growing strain, making the competition between the two strains almost neutral, somewhat enhancing the importance of stochastic effects. Our experiments in time-varying environments show that the existence of thin, persistent filaments can play an important role in determining the outcome of competition between strains. In environments that fluctuate between two environmental states in which each strain has a selective advantage over the other one, the persistent filaments facilitate survival during detrimental environmental states and allow immediate recovery once the relative advantage of the two strains is reversed.

Because the reduced efficiency of natural selection described here is due to physical forces acting within dense cell populations, we believe such effects are relevant for a broad range of biological systems. We expect that the observed reduction in the effective selective advantage of a fitter strain (when sector widths are small) should be relevant for beneficial mutations that arise in a colony and manage to establish a clonal sector. In the initial phase of their dynamics, such sectors will expand at approximately the same rate as the surrounding wild-type cells, and the expansion speed of the beneficial mutation will increase as its sector grows wider. This size-dependent selective advantage of a fitter strain or beneficial mutation is reminiscent of positive frequency-dependent selection (24), in which the fitness of a genotype increases with its frequency in the population. In the context of our work, the frequency dependence is caused by the pressure field induced by cell division. Experimental (25) and theoretical (26) studies have shown that populations undergoing range expansion accumulate deleterious mutations as a result of consecutive founder events and genetic drift being stronger at the frontier in spatial (compared with well-mixed) populations, due to their reduced effective population sizes. Our work suggests that deleterious mutations have higher chances of being maintained in dense, expanding microbial populations than expected based on genetic drift alone, because the effects of differences in fitness are reduced by physical interactions. Our findings are relevant for the fate of drug-resistant mutations that arise in microbial colonies or biofilms. Such mutations are typically associated with fitness deficits. Our work suggests that drug-resistant mutants (e.g., antibiotic-resistant bacteria) emerging in the outer layer of an expanding colony may benefit from the physical interaction with the surrounding wild-type cells and survive for long times in the actively dividing frontier of the colony in the absence of the drugs that they confer resistance to. The application of a drug would reverse the relative fitness of drug-resistant mutants and wild-type cells and allow the drug-resistant mutant to take over the population, similar to our experiments where temperature varies in time for temperature-sensitive strains. We thus expect that the physical interactions between different genotypes investigated here would favor the maintenance of genetic diversity within dense microbial populations and allow such populations to withstand time-dependent fluctuations of the environment or the application of antimicrobial drugs. Finally, our findings may extend beyond microbial populations and inform us about the dynamics of prevascular tumor growth (7, 27). Within tumors, various cell lineages compete for space and form spatially coherent clusters that are reminiscent of the genetic demixing found in colony-growth experiments (28). A recent study (28) has shown that individual tumors can have high levels of genetic diversity and argued that such high-diversity levels can only be explained by non-Darwinian selection, i.e., neutral competition between different clones. The reduced efficiency of natural selection highlighted here is one possible mechanism to explain the apparent neutrality of interclone competition within such tumors.

Methods

Strains. The genotypes of all strains used in this study are reported in *SI Appendix*, Table S1. In fluorescent images, yAG1 is portrayed in blue, yAG2 in yellow, yAG19 in cyan, and yAG20 in magenta. Strains' growth rates were

measured by imaging time-lapse movies of microcolonies of each strain on standard YPD agar plates at 30 °C using an inverted microscope and counting the number of cells in each microcolony at successive time points. The ratio of experimentally measured growth rates $\bar{g}_2/\bar{g}_1 = 1.19 \pm 0.06$ (mean ± SE) was estimated by randomly sampling microcolonies of the two strains, computing their growth rate ratio, and taking the mean across 10^6 random samples.

Colony-Growth Experiments. Colony-growth experiments were conducted on 1% agarose plates with YPD (Yeast extract-Peptone-Dextrose) medium at 30 °C, unless otherwise stated. Plates were poured 2 d before inoculation and stored at room temperature. Strains were pregrown at 30 °C overnight in liquid YPD. Before inoculation on agarose plates, 200 μL of each overnight culture were spun down for 1 min at 9,400 × *g* and resuspended in 1 mL of 1% PBS. The densities of such suspensions were measured with a Coulter Counter and brought to a density of 3×10^7 cells/mL by adding 1% PBS or removing the supernatant in appropriate amounts. If required, suspensions were mixed in the desired ratios. A 0.6 μL droplet was pipetted on each agarose plate.

Sweeping Sectors Dynamics Experiment. We performed two sets of experiments to measure the dynamics of sweeping yAG2 sectors at different growth-layer widths at 30 °C. For the wide-growth-layer experiment, we poured 7 mL YPD 1% agarose medium into 35-mm Petri dishes. After 1 d from pouring, solidified YPD agarose discs were transferred to 100-mm Petri dishes, three discs for each larger dish. One droplet of either a single-strain or a mixed-strain suspension (yAG1 and yAG2 were at a 99–1% frequency) was inoculated on the surface of each disc. To ensure that nutrients did not become depleted, 7 mL of liquid YPD medium were added to the Petri dish and substituted daily. Colonies were imaged twice per day. For the narrow growth layer, we poured 33 mL YPD 1% agarose medium into 100-mm Petri dishes. One droplet of either a single-strain or a mixed-strain suspension (yAG1 and yAG2 were at a 99–1% frequency) was inoculated on the surface of each plate. Colonies were imaged daily.

Radial Expansion Velocities. Single-strain colony radii were measured by fitting circles to each single-strain colony bright-field image. Radial expansion velocities were computed by fitting the radius-vs.-time data to straight lines, separately for each colony. The mean radial expansion velocity of each strain was computed as the mean slope of the radius-vs.-time fits. For the wide-growth-layer experiment, yAG1 and yAG2 expansion velocities were measured across 10 and 9 single-strain colonies, respectively. The mean radii at different times are shown in *SI Appendix*, Fig. S11*A*. The measured velocities were $\bar{v}_1 = 1.89 \pm 0.04$ mm/d (mean ± SD) and $\bar{v}_2 = 2.33 \pm 0.09$ mm/d (mean ± SD). For the narrow-growth-layer experiment, yAG1 and yAG2 expansion velocities were measured across 11 single-strain colonies for each strain. The mean radii at different times are shown in *SI Appendix*, Fig. S11*C*. The measured velocities were $\bar{v}_1 = 1.08 \pm 0.04$ mm/d (mean ± SD) and $\bar{v}_2 = 1.26 \pm 0.04$ mm/d (mean ± SD).

cdc26Δ Mutant Experiments. We performed colony-growth experiments with the strains yAG19 and yAG20 to show that filaments and strain displacements can occur without proliferation of the less-fit strain. These experiments were done with 100-mm Petri dishes filled with 33 mL of 1% agarose YPD medium. We grew single-strain and mixed-strain colonies of yAG19 and yAG20 (yAG19 and yAG20 were at a 5–95% frequency) for 2 d at 28 °C and then moved them to the stage of a stereoscope incubated at 37 °C. Colonies were imaged every 10 min for 23 h. The same experiment was performed with yAG2 and yAG20 single-strain and mixed-strain colonies and the results do not differ qualitatively.

Time-Varying Temperature Experiments. We performed time-varying temperature experiments with 100-mm Petri dishes filled with 33 mL of 1% agarose YPD medium. We inoculated 11 plates with a mixed-strain 0.6 μL droplet (yAG1 and yAG2 were at a 50–50% frequency). Three of these plates were incubated at 30 °C for 2 d, then at 12 °C for 9 d, and then at 30 °C for 14 d (*SI Appendix*, Fig. S3). Three plates were incubated at 30 °C for 3 d, then at 12 °C for 16 d, and then at 30 °C for 10 d (Fig. 2 *A–C* and *SI Appendix*, Fig. S4). Three plates were incubated at 30 °C for 3 d, then at 12 °C for 20 d, and then at 30 °C for 9 d (*SI Appendix*, Fig. S5). One plate was incubated at 30 °C for 13 d and then at 12 °C for 18 d (Fig. 2 *D–L*). We inoculated six plates with a 0.6 μL droplet of yAG1 and another six with yAG2. Three of each strain's plates were stored at room temperature overnight and then moved to a 12 °C incubator for the rest of the experiment. The remaining three plates for each strain were placed in a 30 °C incubator for the entire experiment. We took frequent fluorescent and bright-field images of all plates. Single-strain colonies were used to measure single-strain radial expansion velocities.

Continuum and Constant-Speed Models. The continuum and the constant-speed models were solved numerically (*SI Appendix, Supplementary Methods*) using level-set methods (29) and isotropic discrete operators (30).

ACKNOWLEDGMENTS. A.G. thanks Sauro Succi for helpful discussions on the numerical methods and the Harvard Center for Biological Imaging and Douglas Richardson for helping with the growth rates measurement. We thank the members of the A.W.M. and D.R.N. groups for valuable suggestions. A.G. was supported by research fellowships from the Swiss National Science Foundation, Projects P2ELP2_168498 and P400PB_180823, and work on this project was supported by the Human Frontier Science Program Grant RGP0041/2014 (to A.W.M. and D.R.N.). Work by A.G. and D.R.N. was supported by the National Science Foundation, via Grant DMR1608501 and via the Harvard Materials Science Research and Engineering Center via Grant DMR1435999.

1. Crow JF, Kimura M (2009) *An Introduction to Population Genetics Theory* (Blackburn Press, Caldwell, NJ).
2. Hallatschek O, Hersen P, Ramanathan S, Nelson DR (2007) Genetic drift at expanding frontiers promotes gene segregation. *Proc Natl Acad Sci USA* 104:19926–19930.
3. Hallatschek O, Nelson DR (2009) Population genetics and range expansions. *Phys Today* 62:42–47.
4. Hallatschek O, Nelson DR (2010) Life at the front of an expanding population. *Evolution* 64:193–206.
5. Korolev KS, et al. (2012) Selective sweeps in growing microbial colonies. *Phys Biol* 9: 026008.
6. Weinstein BT, Lavrentovich MO, Möbius W, Murray AW, Nelson DR (2017) Genetic drift and selection in many-allele range expansions. *PLoS Comput Biol* 13:e1005866.
7. Lavrentovich MO, Nelson DR (2015) Survival probabilities at spherical frontiers. *Theor Popul Biol* 102:26–39.
8. Kimura M, Weiss GH (1964) The stepping stone model of population structure and the decrease of genetic correlation with distance. *Genetics* 49:561–576.
9. Excoffier L, Foll M, Petit RJ (2009) Genetic consequences of range expansions. *Annu Rev Ecol Evol Syst* 40:481–501.
10. Müller MJI, Neugeboren BI, Nelson DR, Murray AW (2014) Genetic drift opposes mutualism during spatial population expansion. *Proc Natl Acad Sci USA* 111: 1037–1042.
11. Van Dyken JD, Müller MJI, Mack KML, Desai MM (2013) Spatial population expansion promotes the evolution of cooperation in an experimental Prisoner's dilemma. *Curr Biol* 23:919–923.
12. Weber MF, Poxleitner G, Hebisch E, Frey E, Opitz M (2014) Chemical warfare and survival strategies in bacterial range expansions. *J R Soc Interface* 11:20140172.
13. Nadell CD, Drescher K, Foster KR (2016) Spatial structure, cooperation and competition in biofilms. *Nat Rev Microbiol* 14:589–600.
14. Giometto A, Rinaldo A, Carrara F, Altermatt F (2014) Emerging predictable features of replicated biological invasion fronts. *Proc Natl Acad Sci USA* 111:297–301.
15. Giometto A, Altermatt F, Rinaldo A (2017) Demographic stochasticity and resource autocorrelation control biological invasions in heterogeneous landscapes. *Oikos* 125: 1554–1563.
16. Korolev KS, Avlund M, Hallatschek O, Nelson DR (2010) Genetic demixing and evolution in linear stepping stone models. *Rev Mod Phys* 82:1691–1718.
17. McNally L, et al. (2017) Killing by Type VI secretion drives genetic phase separation and correlates with increased cooperation. *Nat Commun* 8:14371.
18. Farrell FD, Gralka M, Hallatschek O, Waclaw B (2017) Mechanical interactions in bacterial colonies and the surfing probability of beneficial mutations. *J R Soc Interface* 14:20170073.
19. Kayser J, Schreck C, Gralka M, Fusco D, Hallatschek O (2018) Collective motion conceals fitness differences in crowded cellular populations. bioRxiv:10.1101/267286.
20. Hwang LH, Murray AW (1997) A novel yeast screen for mitotic arrest mutants identifies DOC1, a new gene involved in cyclin proteolysis. *Mol Biol Cell* 8:1877–1887.
21. Singh A, Manney TR (1974) Genetic analysis of mutations affecting growth of Saccharomyces cerevisiae at low temperature. *Genetics* 77:651–659.
22. Klapper I, Dockery J (2002) Finger formation in biofilm layers. *SIAM J Appl Math* 62: 853–869.
23. Batchelor GK (2000) *An Introduction to Fluid Dynamics* (Cambridge Univ Press, Cambridge, UK).
24. Prout T (2001) Frequency-dependent selection. *Encyclopedia of Genetics*, eds Brenner S, Miller JH (Academic, San Diego), Vol 1, pp 730–731.
25. Bosshard L, et al. (2017) Accumulation of deleterious mutations during range expansions. *Genetics* 207:669–684.
26. Peischl S, Dupanloup I, Kirkpatrick M, Excoffier L (2013) On the accumulation of deleterious mutations during range expansions. *Mol Ecol* 22:5972–5982.
27. Korolev KS, Xavier JB, Gore J (2014) Turning ecology and evolution against cancer. *Nat Rev Cancer* 14:371–380.
28. Ling S, et al. (2015) Extremely high genetic diversity in a single tumor points to prevalence of non-Darwinian cell evolution. *Proc Natl Acad Sci USA* 112:E6496–E6505.
29. Osher S, Fedkiw RP (2003) *Level Set Methods and Dynamic Implicit Surfaces* (Springer, New York).
30. Thampi SP, Ansumali S, Adhikari R, Succi S (2013) Isotropic discrete Laplacian operators from lattice hydrodynamics. *J Comput Phys* 234:1–7.